

Language as a Wave Phenomenon: Iso-Energetic Phase-Locking and Semantic Interference in Neural Networks

Alper YILDIRIM ¹ and İbrahim YÜCEDAĞ ¹

¹Department of Computer Engineering, Düzce University, Turkey

Abstract

Conventional deep learning paradigms rely on metabolically expensive magnitude-based representations, rendering them fundamentally incompatible with passive photonic hardware. We introduce PRISM, a sequence modeling architecture that bridges high-level reasoning and physical constraints by enforcing an Iso-Energetic (Unity Gain) principle, compelling the network to encode semantic information exclusively in the phase angle. Validated on the WMT14 translation benchmark, PRISM achieves a 0.799 COMET score, demonstrating that phase-based reasoning competes with standard Transformers (0.821) and functionally matches unconstrained spectral baselines like FNet (0.805), despite enforcing strict energy constraints and requiring 11.5% fewer parameters. Furthermore, to verify hardware feasibility, we simulate a Holographic Backpropagation mechanism on a noisy, 4-bit optical correlator. Ablation studies reveal a substantial performance gain (48.4% vs. 62.4%) over a frozen baseline, proving that the proposed phase-steering mechanism actively optimizes physical parameters under strict energy constraints. These results establish an existence proof that ultra-low-power, passive optical hardware can support high-level linguistic intelligence without sacrificing representational capacity.

Keywords: Optical Neural Networks, Phase Coding, Photonic Computing, Complex-Valued Deep Learning, Spectral Reasoning, Iso-Energetic Constraints, Neuromorphic NLP, Holographic Learning.

1 Introduction

A fundamental disparity exists between biological and artificial intelligence: the cost of computation. While the human cortex processes complex language using approximately 20 watts of power (Laughlin and Sejnowski, 2003), state-of-the-art Large Language Models require kilowatts. This physical inefficiency is rooted in a deeper algorithmic inefficiency: the reliance on *Rate Coding*.

In the Rate Coding paradigm (standard Transformers), information importance is encoded in the *magnitude* of activation vectors (Vaswani et al., 2017). To differentiate signal from noise, the network must effectively “shout”—amplifying specific features to high values while suppressing others. On digital hardware, this manifests as dense matrix multiplications; in biological terms, this is metabolically ruinous. While recent State Space Models such as Mamba (Gu and Dao, 2024) have successfully reduced computational complexity to linear time, they largely retain this underlying magnitude-based representational paradigm.

Author Contributions: A. Yildirim designed the PRISM architecture, implemented the codebase, and conducted the experimental validation. Prof. Dr. I. Yucedag provided academic supervision and mentorship.

Neuroscience suggests an alternative paradigm: *Phase Coding*. Unlike the “shouting” mechanism of rate coding, biological circuits utilize oscillatory synchronization to bind semantic features by their relative timing (phase angle) without increasing firing rates (Fries, 2005). By enforcing an **Iso-Energetic Constraint** (Unity Gain), the brain essentially decouples semantic processing from signal energy—a mechanism hypothesized to be fundamental to cortical speech processing (Giraud and Poeppel, 2012). Recent theoretical frameworks, such as the Weakly Coupled Oscillator (WCO-TS) model (Dogonasheva et al., 2025), further propose that “Transient Synchronization” is the primary mechanism for recognition.

However, a critical architectural gap remains for long-sequence modeling. State Space Models (SSMs) like Mamba are inherently recurrent and causal, making them suboptimal for tasks requiring global, bidirectional context—such as identifying distal regulatory elements in genomic sequences. While Transformers offer bidirectionality, their quadratic complexity precludes scaling to chromosomal lengths. PRISM addresses this by offering global mixing via the Fast Fourier Transform (FFT) with linearithmic complexity.

While complex-valued neural networks have been proposed for NLP, they have historically faced two limitations. First, early oscillatory models were restricted to “toy” domains like synthetic wave classification (Hopfield and Brody, 2001). Second, recent attempts to scale complex-valued embeddings to translation tasks (Wang et al., 2020) have relied on unstable learnable frequencies and retained the energy-intensive, quadratic Attention mechanism to mix information. It has remained unproven whether a purely *spectral*, attention-free architecture is robust enough to handle the high-dimensional, ambiguous nature of human language.

In this work, we bridge this gap by scaling biological constraints to an industrial benchmark. We introduce the Phase-Resonant Intelligent Spectral Model (PRISM), an architecture that replaces the Attention mechanism with complex-valued Gated Harmonic Convolutions. We enforce a strict **Iso-Energetic Constraint** (Gain ≈ 1.0), compelling the network to solve the WMT14 German-to-English translation task using *only* phase manipulation. Crucially, we introduce **Rotary Semantic Embeddings (RoSE)**, which stabilize training by replacing learned frequencies with fixed geometric rotations, effectively creating a parameter-free coordinate system for semantic meaning.

To our knowledge, this is the first demonstration of a **strict Iso-Energetic Spectral system** achieving competitive performance on a standard NLP benchmark. We compare PRISM against a Rate-Coding Control Group (ROPE Transformer) and find that despite being metabolically constrained and structurally lighter, the Phase-Coding model achieves comparable fidelity (0.799 COMET (Rei et al., 2022) for the efficient Tied configuration vs 0.821 COMET). This result serves as an existence proof: the efficient, wave-based mechanisms of the brain are not limiting constraints, but optimal computational solutions capable of supporting general intelligence at scale.

2 Architecture

We formally define the Phase-Resonant Intelligent Spectral Model (PRISM), a sequence modeling paradigm rooted in wave mechanics. Unlike standard Transformers which treat tokens as static vectors manipulated by additive updates, PRISM treats tokens as complex phasors $z = re^{i\theta}$, where semantic identity is encoded in the angle θ and signal intensity in the magnitude r .

2.1 Rotary Semantic Embeddings (RoSE)

We introduce Rotary Semantic Embeddings (RoSE) to unify semantic identity and positional context into a single complex-valued phasor. Unlike standard architectures that add positional encodings to

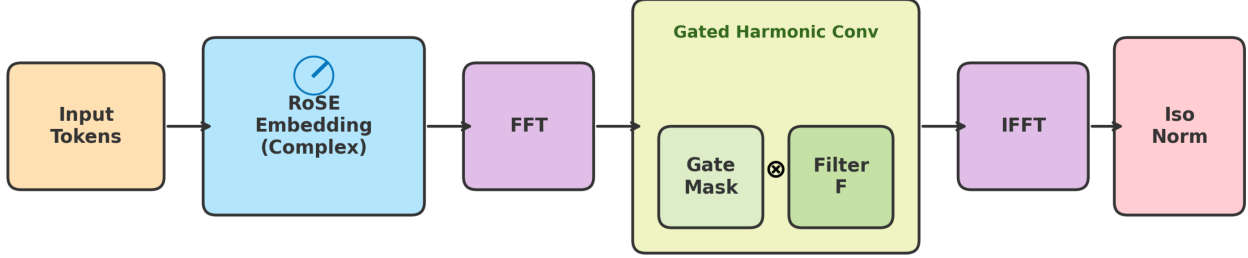


Figure 1: The PRISM Architecture. (Left) Input tokens are encoded as complex phasors via RoSE. (Center) Gated Harmonic Convolutions replace $\mathcal{O}(N^2)$ attention with $\mathcal{O}(N \log N)$ spectral filters \mathbf{H} . (Right) Iso-Energetic Norm enforces unit gain ($g \approx 1.0$), forcing semantic encoding into phase shifts.

static embeddings ($e + p$), RoSE operates via multiplicative rotation in the complex plane.

Let w_t be the token at position t . We first project w_t into a complex latent space \mathbb{C}^d by learning separate real and imaginary components, forming a content vector $z_t \in \mathbb{C}^d$. To encode position, we define a spectrum of geometric frequencies $\omega \in \mathbb{R}^d$, distributed logarithmically to capture multi-scale dependencies:

$$\omega_k = \frac{1}{10000^{k/d}}, \quad k \in [0, d - 1] \quad (1)$$

The final embedding $E(w_t)$ is obtained by rotating the content vector z_t by the positional phase angle:

$$E(w_t) = z_t \cdot e^{i\omega t} \quad (2)$$

This formulation ensures that the relative distance between tokens t and $t + k$ is preserved as a constant phase shift $e^{i\omega k}$ in the frequency domain, providing a natural inductive bias for sequence modeling.

2.2 Gated Harmonic Convolution

The core reasoning unit of PRISM is the Gated Harmonic Convolution. Unlike recent ‘‘Holographic’’ architectures which introduce phase dynamics but retain the quadratic computational cost of pairwise attention (Huang et al., 2025), PRISM replaces the attention mechanism entirely. This layer filters information in the frequency domain ($\mathcal{O}(N \log N)$) while allowing the time-domain signal to dynamically modulate its own phase and magnitude.

Given a sequence of complex embeddings $\mathbf{X} \in \mathbb{C}^{L \times d}$, we first normalize the input using Phase-Preserving Layer Normalization. We then compute two separate data-dependent gates, $\mathbf{G}_{re} \in \mathbb{R}^{L \times d}$ and $\mathbf{G}_{im} \in \mathbb{R}^{L \times d}$, using the concatenated real and imaginary components of the normalized input $\tilde{\mathbf{X}}$:

$$[\mathbf{G}_{re} \parallel \mathbf{G}_{im}] = \sigma \left(\mathbf{W}_{gate} [\text{Re}(\tilde{\mathbf{X}}) \parallel \text{Im}(\tilde{\mathbf{X}})] \right) \quad (3)$$

Simultaneously, we transform the sequence into the frequency domain via the Fast Fourier Transform (FFT) and apply a learnable global filter $\mathbf{H} \in \mathbb{C}^{L \times d}$. This spectral filtering mirrors the biological phenomenon of ‘‘Connectome Harmonics’’ (Atasoy et al., 2016; Deco et al., 2025), where brain dynamics naturally self-organize into standing waves (eigenmodes) to integrate information efficiently. This operation is mathematically dual to the Selective State Space mechanism utilized in efficient engineering models like Mamba, demonstrating a convergent evolution between biological spectral gating and hardware-optimized linear recurrence.

$$\mathbf{Y}_{freq} = \text{FFT}(\tilde{\mathbf{X}}) \odot \mathbf{H} \quad (4)$$

The filtered signal is returned to the time domain via the Inverse FFT (IFFT). Crucially, we apply **Cartesian Gating**, where the real and imaginary components are modulated independently:

$$\mathbf{Y}_{out} = \text{Re}(\text{IFFT}(\mathbf{Y}_{freq})) \odot \mathbf{G}_{re} + i \cdot (\text{Im}(\text{IFFT}(\mathbf{Y}_{freq})) \odot \mathbf{G}_{im}) \quad (5)$$

Unlike scalar gating which only scales magnitude, this independent Cartesian modulation allows the network to alter the phase angle $\theta = \arctan(\text{Im}/\text{Re})$ of the latent vectors, enabling the "Contextual Phase Steering" mechanism described in Section 4.

2.3 Phase-Preserving Non-Linearity (ModReLU)

Standard activation functions like ReLU are ill-defined for complex numbers as they destroy phase information. We adopt ModReLU, which rectifies the magnitude of the complex vector while strictly preserving its phase angle. For a complex input z :

$$\text{ModReLU}(z) = \text{ReLU}(|z| + b) \cdot \frac{z}{|z|} \quad (6)$$

where b is a learnable bias parameter. This ensures that the semantic orientation of the vector (its "meaning") remains unchanged, while its intensity (magnitude) is non-linearly scaled.

2.4 Holomorphic Dropout

To prevent the network from over-relying on specific frequency bands, we introduce Holomorphic Dropout. Unlike standard dropout which operates on scalars, applying independent masks to the real and imaginary components would destroy the phase angle θ . Instead, we sample a single binary mask $m \sim \text{Bernoulli}(1 - p)$ and apply it identically to both components:

$$z_{drop} = (m \cdot \text{Re}(z)) + i \cdot (m \cdot \text{Im}(z)) \quad (7)$$

This ensures that if a feature is dropped, its entire spectral contribution (amplitude and phase) is removed simultaneously, forcing the network to distribute semantic information holographically across the spectrum.

2.5 Phase-Preserving Layer Normalization

To maintain the stability of the complex gradients, a critical challenge in high-dimensional complex manifolds (Trabelsi et al., 2018), we utilize a normalization scheme that operates solely on the magnitude. Given a vector z , we compute the mean μ and variance σ^2 of its magnitude $|z|$:

$$\text{PPLN}(z) = \frac{z}{|z|} \cdot \frac{|z| - \mu}{\sqrt{\sigma^2 + \epsilon}} \cdot \gamma + \beta \quad (8)$$

This decouples the signal's energy from its phase, reinforcing the Iso-Energetic reasoning regime. This aligns with the theoretical advantages of Unitary Recurrent Networks (Arjovsky et al., 2016), where strictly preserving the norm of the hidden state (Gain ≈ 1) prevents the vanishing gradient problem inherent in complex-valued optimization.

2.6 Complex-to-Real Bridge

To interface the complex-valued PRISM encoder with the real-valued standard Transformer decoder, we introduce a projection bridge. The complex state z_{enc} is mapped to the real domain \mathbb{R}^d by concatenating its components and projecting via a linear layer \mathbf{W}_{bridge} :

$$h_{real} = \text{LN}(\mathbf{W}_{bridge}[\text{Re}(z_{enc}) \parallel \text{Im}(z_{enc})]) \tag{9}$$

This bridge compresses the spectral phase information into a dense real-valued representation suitable for cross-attention.

3 Methodology

3.1 Dataset and Preprocessing

To validate the spectral reasoning capabilities of PRISM, we utilize the WMT14 German-to-English translation dataset (Bojar et al., 2014), a standard benchmark for sequence-to-sequence modeling established by the statistical machine translation community and popularized by Vaswani et al. (2017). Tokenization is performed using the pre-trained tokenizer from the Helsinki-NLP OPUS-MT model Tiedemann and Thottingal (2020). Our preliminary analysis of the corpus distribution revealed that sequences exceeding 128 tokens constitute less than 1% of the dataset. Consequently, we apply a hard filtering threshold, discarding samples with lengths $L > 128$. This truncation retains over 99% of the training data while significantly reducing the computational overhead associated with processing extreme outliers. To further optimize training throughput, we implement dynamic bucketing with a width of 4 and a target bucket size of 20,000 tokens. This strategy groups sequences of similar lengths, minimizing the padding ratio within each training batch and stabilizing the spectral gradients.

3.2 Experimental Design: Phase-Coding vs. Rate-Coding Regimes

To isolate the computational sufficiency of wave-based reasoning, we utilize the WMT14 dataset. While PRISM is ultimately intended for long-range biological sequences (e.g., Genomics), natural language serves as a superior testbed for mechanism validation. Its inherent semantic structure (synonyms, antonyms) allows us to explicitly verify if ‘Phase Coding’ can capture relationship dynamics in a way that raw DNA classification accuracy cannot.

We establish a comparative study between two distinct neural regimes. The **Control Group (Rate-Coding)** is a standard Transformer (Vaswani et al., 2017) representing the unconstrained, energy-intensive magnitude paradigm. The **Experimental Group (Phase-Coding)** is the PRISM architecture, constrained by the Iso-Energetic Unity Gain principle. Both models are configured with a 6-layer encoder and a 6-layer decoder, and are trained using Pre-Layer Normalization (Pre-LN) (Nguyen and Salazar, 2019) to ensure gradient stability at depth.

The Control Group utilizes Rotary Position Embeddings (RoPE) (Su et al., 2024), allowing it to encode position via rotation while retaining the freedom to encode semantics via magnitude.

Spectral Baseline (FNet): To isolate the benefits of spectral mixing from the constraints of phase coding, we include an FNet baseline (Lee-Thorp et al., 2022). Unlike PRISM, FNet utilizes a real-valued FFT for token mixing without energy restrictions. A critical limitation of FNet is the dependence of its learned filters on specific frequency bins defined by sequence length N . Dynamic variation of N destabilizes training; consequently, while PRISM utilizes dynamic bucketing, the FNet baseline was trained using **fixed-length batches** ($L = 128$) to ensure spectral consistency.

Experimental Fairness: Despite the difference in padding strategies, we ensured strict parity in the learning curriculum. We synchronized the **effective batch size** ($\approx 20,000$ tokens) and the **total count of meaningful training tokens** across all models by adjusting gradient accumulation steps dynamically. This guarantees that the FNet baseline was exposed to the exact same semantic signal volume and optimization noise profile as PRISM, isolating the architecture as the sole variable.

Capacity Balancing: Since the standard FNet layer lacks learnable mixing weights (relying on parameter-free FFTs), a standard 6-layer configuration would result in fewer parameters than PRISM. To ensure a rigorous comparison where the baseline is not disadvantaged by parameter scarcity, we increased the FNet encoder depth to **7 layers** (vs. 6 for PRISM). This establishes a baseline with significantly higher total capacity (14.7M vs. 13.0M), ensuring that PRISM’s efficiency is demonstrated against a structurally superior control group. Furthermore, to strictly isolate the impact of the encoder architecture, the FNet model utilized the exact same RoPE-augmented Transformer Decoder as the Control and Experimental groups.

In contrast, the Experimental Group (PRISM) employs Rotary Semantic Embeddings (RoSE), forcing both position and semantics to compete for bandwidth exclusively in the phase domain.

A distinct characteristic of the PRISM architecture is the redistribution of parameter density from "logic" (feed-forward networks and attention) to "memory" (embeddings). As detailed in Table 1, PRISM achieves a highly efficient profile, requiring only **69.1M parameters** compared to the Standard Transformer’s **73.8M**. Crucially, the spectral reasoning core is significantly lighter: **6-Layered PRISM Encoder requires 31.2% fewer parameters** than the standard 6-Layered Self-Attention encoder (13.0M vs 18.9M).

1. **PRISM-Standard (Tied):** The mathematically efficient form where output weights are tied to the input embeddings ($\mathbf{W}_{out} = \mathbf{W}_{emb}^T$). As shown in Table 1, this configuration surpasses the density of standard Transformers.
2. **PRISM-Large (Untied):** The untied experimental form used for **comparative capacity analysis**. To maximize potential translation fidelity, this variant decouples the input and output spaces, increasing the total parameter count to approximately **99M**.

Consequently, the performance results (0.799 COMET, 27.6 BLEU) are derived from the **PRISM-Standard (Tied)** configuration, demonstrating that the architectural efficiency highlighted in Table 1 is achievable without compromising translation fidelity. While PRISM’s primary utility

Table 1: **Architectural Configurations.** Comparison of parameter distribution including the spectral FNet baseline. PRISM (Tied) achieves the lowest parameter footprint, reducing encoder density by $> 10\%$ compared to FNet while adding physical constraints.

Component	Transformer	FNet	PRISM (Tied)	PRISM (Untied)
EMBEDDINGS	29.7M	30.3M	30.3M	89.2M
ENCODER	18.9M	14.7M	13.0M	13.4M
BRIDGE	0.0M	0.5M	0.5M	0.5M
DECODER	25.2M	25.2M	25.2M	25.2M
Total	73.8M	71.2M	69.1M	128.4M

lies in bidirectional encoding for long-context tasks (e.g., genomic classification), we adopted a Sequence-to-Sequence (Encoder-Decoder) framework for this initial validation. This choice was driven by two factors. First, the Complex-to-Real Bridge acts as a statistical stabilizer, normalizing the high-variance spectral features of the complex encoder before they enter the generation phase.

Second, utilizing a standard real-valued Transformer decoder isolates the experimental variable (Phase Coding) to the reasoning stage, ensuring that any instability in generation can be attributed to the encoder’s representation rather than the decoding mechanism itself. This hybrid design serves as a robust ‘first prototype’ for validating complex-valued harmonics in a controlled environment.

3.3 Training Configuration

All models were optimized using AdamW (Loshchilov and Hutter, 2019), the variant of Adam (Kingma and Ba, 2015), with default PyTorch parameters with weight decay of 0.01. We employed a cosine learning rate schedule with a warmup of 600 steps.

To ensure fair comparison, learning rates were tuned individually for stability and performance. The **PRISM-Untied** model was trained with a peak learning rate of $8 \cdot 10^{-4}$. However, the **Standard Transformer** (Control Group) exhibited gradient instability at this magnitude; consequently, the Transformer, FNet and the **PRISM-Tied** configuration were trained with a reduced peak learning rate of $6 \cdot 10^{-4}$ to ensure stable convergence.

Global batch size was maintained at approximately 20,000 tokens via gradient accumulation. To preserve the spectral fidelity of the complex-valued gradients and prevent phase collapse, we utilized Single Precision (FP32) training with hardware-accelerated matrix multiplication. We explicitly avoided standard Mixed-Precision (FP16) to mitigate the risk of catastrophic cancellation in the harmonic convolutional layers.

3.4 Hardware Validation: Holographic Optical Learning

While PRISM demonstrates spectral reasoning capacity on WMT14, a core theoretical motivation for this architecture is its compatibility with passive photonic hardware. To validate this beyond theoretical hypothesis, we constructed a differentiable simulation of a standard 4f-Correlator optical system Goodman (2005), adapting the physical error-backpropagation frameworks established in diffractive deep neural networks Lin et al. (2018).

3.4.1 The Holographic Gradient Principle

In standard digital backpropagation, gradients are computed symbolically. However, in a physical wave-based system, the weight update can be realized through the interference of the forward-propagating signal wave (E_{fwd}) and the backward-propagating error wave (E_{bwd}). This corresponds to the principle of *Holographic Recording*, mathematically expressed as the interference term in the complex plane, a mechanism analogous to the in-situ training of diffractive optical layers Lin et al. (2018); Wagner and Psaltis (1987).

$$\Delta\Phi \propto \text{Re}(E_{fwd} \cdot E_{bwd}^*) \tag{10}$$

where E_{bwd}^* represents the phase-conjugate (time-reversed) error signal. We implemented this update rule to verify that the network can self-optimize using local wave interference rather than global digital memory.

3.4.2 Hardware-Aware Simulation Constraints

To ensure the experiment reflects the reality of a low-power analog optical co-processor, rather than an idealized digital approximation, we enforce three strict physical constraints:

1. **Square-Law Detection:** Optical sensors measure intensity ($I \propto |E|^2$), not amplitude. We incorporated a square-law detection layer, forcing the network to solve the "Phase Retrieval" problem implicitly during the learning process.
2. **Iso-Energetic Transmission:** The optical layer (SLM) is constrained to a unity-gain regime (Gain ≈ 1.0), preventing the model from relying on signal amplification (Rate Coding).
3. **Stochastic Detector Noise:** To simulate physical sensor imperfections and thermal fluctuations, we inject multiplicative intensity noise ($\sigma \approx 0.01$) during the training phase. This ensures the model learns robust features that are resilient to signal degradation in the optical readout layer.

We conduct an ablation study on the CIFAR-10 dataset (Krizhevsky et al., 2009), comparing a *Learned Optical Layer* against a *Frozen (Random) Optical Layer* to quantify the specific contribution of holographic learning.

4 Mechanistic Analysis Methodology

To investigate the internal reasoning dynamics of the PRISM architecture, we introduce the **Dual-Regime Spectral Probe**, a mechanistic framework designed to disentangle structural filtering from semantic reasoning. Unlike standard attention map analysis, which measures pairwise importance, our approach quantifies the physical transformation of token embeddings in the frequency domain. **Model Selection for Analysis:** While the *Tied* configuration achieves slightly higher aggregate performance (0.799 COMET), we conduct our mechanistic analysis on the **PRISM-Large (Untied)** variant (0.797 COMET). This separates the input and output embedding spaces, ensuring that the phase dynamics we observe are driven by *reasoning* (deep layers) rather than the geometric constraints of a shared embedding lookup table.

4.1 Experimental Setup: The Dual-Regime Dataset

We curate a rigorous evaluation dataset consisting of paired sentences, strictly filtered to ensure all target concepts map to single tokens in the BPE vocabulary. This prevents sub-word tokenization artifacts from contaminating the phase measurements. We define two distinct semantic regimes:

The Inertial Regime (Control Group): A set of $N = 30$ high-frequency, unambiguous concepts (e.g., "Katze" (Cat), "Sonne" (Sun)) embedded in simple declarative contexts (labeled **Easy** in Table 4). This regime establishes the model's "resting state," measuring the baseline spectral distortion applied to tokens that require no disambiguation.

The Steering Regime (Stress Test): A set of $N = 28$ polysemous instances (e.g., "Bank" (Finance/Bench), "Schloss" (Castle/Lock), "Leiter" (Ladder/Leader)) (labeled **Hard** in Table 4). This regime forces the model to actively resolve semantic ambiguity, isolating the specific computational work required for disambiguation.

4.2 Physical Metrics

We instrument the network with forward hooks to capture the input vector $x^{(l)}$ and output vector $y^{(l)}$ at each layer l . We define three primary physical metrics:

1. Iso-Energetic Gain (g): To test the hypothesis that the network operates as a Frequency Modulation (FM) system, we measure the signal amplitude amplification ratio. A value of $g \approx 1.0$ indicates an iso-energetic carrier wave, whereas $g \gg 1.0$ would indicate Amplitude Modulation (AM).

$$g^{(l)} = \frac{\|y^{(l)}\|_2}{\|x^{(l)}\|_2 + \epsilon} \quad (11)$$

2. Effective Phase Rotation ($\Delta\theta$): Since the PRISM encoder operates in the complex domain, we quantify semantic transformation as the effective angular displacement between the input and output phasors. We compute the cosine similarity in the complex plane and convert it to degrees:

$$\Delta\theta^{(l)} = \arccos\left(\frac{\text{Re}(\langle x^{(l)}, y^{(l)} \rangle)}{\|x^{(l)}\|_2 \|y^{(l)}\|_2}\right) \cdot \frac{180}{\pi} \quad (12)$$

This metric serves as a proxy for "semantic work," representing how aggressively the layer steers the representation in the latent space.

3. Distributional Topology (Skewness): Beyond mean values, we analyze the shape of the rotation distribution to detect selective reasoning. We calculate the sample skewness γ_1 of the rotation angles $\Theta = \{\Delta\theta_1, \dots, \Delta\theta_n\}$:

$$\gamma_1 = \frac{\frac{1}{n} \sum_{i=1}^n (\Delta\theta_i - \bar{\theta})^3}{\left(\frac{1}{n} \sum_{i=1}^n (\Delta\theta_i - \bar{\theta})^2\right)^{3/2}} \quad (13)$$

A near-zero skewness ($\gamma_1 \approx 0$) implies a uniform, predictable transformation applied to all tokens. A high positive skewness ($\gamma_1 > 1.0$) indicates a "heavy-tailed" process, where the model exerts extreme effort on a small subset of tokens (the "Long Neck") while leaving the majority unmodified (the "Fat Bottom").

5 Quantitative & Qualitative Results

We evaluate PRISM on two fronts: translation performance and mechanistic interpretability. As shown in Table 2, PRISM (0.799 COMET) effectively matches the performance of the unconstrained spectral FNet baseline (0.805 COMET), despite the latter operating with real-valued amplitude freedom. While the standard Transformer retains a slight lead (0.821 COMET), our primary contribution is the identification of distinct physical phenomena governing the model’s latent space.

Table 2: **WMT14 Translation Performance.** PRISM achieves near-parity with the unconstrained FNet baseline despite enforcing the Iso-Energetic constraint and using fewer parameters. The performance gap indicates that "Amplitude" (Rate Coding) provides diminishing returns for spectral models.

Model	Params (Enc)	Constraint	BLEU	COMET
TRANSFORMER	18.9M	RATE (ACTIVE)	28.4	0.821
FNET (BASE)	14.7M	RATE (FIXED)	28.2	0.805
PRISM	13.0M	Phase (Iso)	27.6	0.799

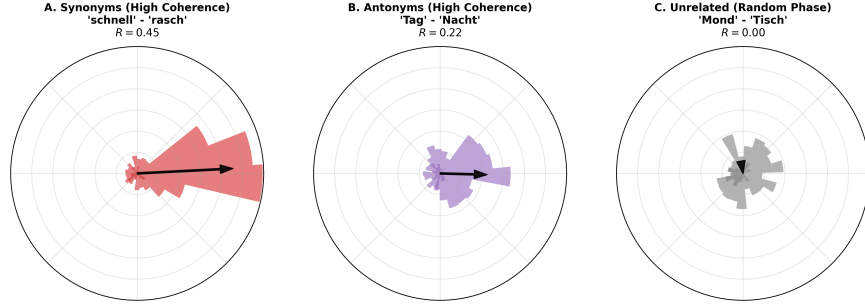


Figure 2: **The Semantic Phase Compass.** Distribution of phase differences $\Delta\theta$ for three representative pairs. **(A) Synonyms** exhibit strong phase locking, indicating constructive interference. **(B) Antonyms** also show high coherence, confirming a shared spectral basis. **(C) Unrelated words** display a uniform, random phase distribution.

5.1 Static Structure: Neural Phase Locking

To validate the hypothesis that PRISM encodes semantic proximity as geometric alignment, we analyze the *Weighted Mean Resultant Length* (R) of the phase difference vectors between word pairs. For a pair of token embeddings $\mathbf{z}_a, \mathbf{z}_b \in \mathbb{C}^d$, we weight the phase coherence by the signal energy in each frequency band k . R is defined as:

$$R = \left| \frac{\sum_{k=1}^d |\mathbf{z}_{a,k}| |\mathbf{z}_{b,k}| e^{i\Delta\phi_k}}{\sum_{k=1}^d |\mathbf{z}_{a,k}| |\mathbf{z}_{b,k}|} \right| \quad (14)$$

where $\Delta\phi_k = \text{Angle}(\mathbf{z}_{a,k}) - \text{Angle}(\mathbf{z}_{b,k})$ is the phase difference at frequency k . Here, $R \in [0, 1]$ quantifies angular coherence. We note that due to the strict Iso-Energetic constraint enforcing unity gain ($|\mathbf{z}| \approx 1.0$), the weighting terms $|\mathbf{z}_{a,k}| |\mathbf{z}_{b,k}|$ approach unity, effectively reducing this metric to the standard unweighted circular mean.

Table 3: **Phase Coherence Statistics.** Synonyms show the highest phase locking, followed by Antonyms. Random pairs define the noise floor ($R < 0.08$). See Appendix A for full distribution details.

Category	Mean $R \pm$ Std	Count
Synonym	0.198 ± 0.090	35
Antonym	0.117 ± 0.057	13
Random	0.077 ± 0.031	19

As illustrated in Figure 2 and Table 3, we observe a distinct regime of *Neural Phase Locking*. Synonymous pairs align their spectral components to maximize interference, yielding high R values. Crucially, antonyms also maintain high phase coherence (0.117), distinguishing themselves from random noise (0.077). This supports that the RoSE embedding space is topologically structured, where "meaning" is determined by the harmonic signature of the token rather than simple Euclidean distance.

5.2 Dynamic Inference: The "Steering" Hypothesis

While the Phase Compass demonstrates that static embeddings are structured, it does not explain how the model resolves ambiguity during inference. To investigate this, we instrumented the network

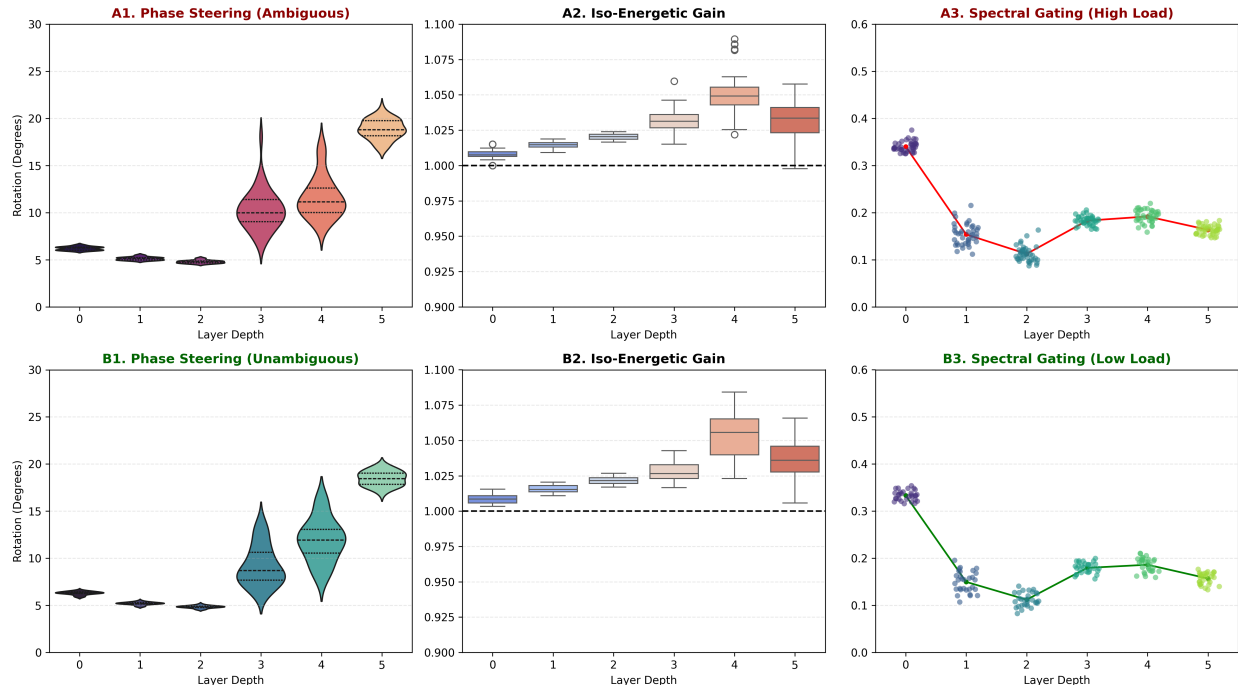


Figure 3: **The Dual-Regime Inference Dashboard.** (Left) **Iso-Energetic Regime:** Signal gain remains strictly near unity ($g \approx 1.0$) across all layers, forcing information processing into the phase domain. (Center) **Inertial Baseline:** Unambiguous tokens (Blue) follow a Gaussian rotation profile with low skewness. (Right) **Selective Steering:** Polysemous tokens (Red) exhibit a heavy-tailed distribution (Skewness > 4.7), suggesting that the network exerts "computational work" only when necessary.

with the **Dual-Regime Probe**, subjecting it to both unambiguous control sentences ("Easy Mode") and high-entropy polysemous contexts ("Hard Mode").

The Iso-Energetic Baseline. First, we observe that the signal gain is strictly constrained to unity ($g \approx 1.0$) across all layers and regimes. This constraint mirrors the directional optimization principles of von Mises-Fisher loss (Kumar and Tsvetkov, 2019), where semantic density is strictly confined to the unit hypersphere surface. Consequently, the network is effectively precluded from using amplitude modulation (AM) for feature selection, forcing it to rely exclusively on phase modulation (FM).

Selective Phase Steering. Table 4 reveals the core reasoning mechanism of the architecture. In the early layers (0-2), both regimes exhibit identical, low-skew behavior, suggesting a uniform "encoding" phase. This mirrors the hierarchical emergence of linguistic features observed in standard Transformers (Tenney et al., 2019), where lower layers process local syntax before higher layers resolve complex semantics. However, unlike standard models, a significant bifurcation occurs in the deep layers (3-5) driven entirely by phase dynamics.

In Layer 5, the **Mean Rotation** for both regimes is nearly identical (18.47° vs 18.92°). This implies that the "average" semantic distance traveled by a token is similar, likely driven by the layer's fixed spectral filter structure.

However, the **Distributional Topology** tells a different story. The Easy regime maintains a

Table 4: **The Dual-Regime Divergence.** Comparison of phase rotation dynamics between the Inertial (Easy) and Steering (Hard) regimes. Note that while the **Mean** rotation remains stable across both regimes ($\Delta < 0.5^\circ$), the **Skewness** diverges violently in deeper layers. The explosion of Skewness to **4.71** in Layer 5 provides strong evidence that PRISM exerts "semantic work" selectively, applying extreme rotations ($\Delta\theta_{max} \approx 35^\circ$) only to polysemous tokens.

Layer	Mean Rotation		Max Rotation		Distribution Skew	
	Easy	Hard	Easy	Hard	Easy	Hard
0	6.31°	6.06°	6.61°	6.56°	-0.80	-1.35
1	5.20°	5.01°	5.51°	5.49°	-0.55	-1.18
2	4.85°	4.69°	5.17°	5.17°	-0.27	-0.96
3	9.20°	10.07°	13.82°	18.05°	0.73	1.03
4	11.91°	11.27°	16.34°	17.38°	0.16	0.81
5	18.47°	18.92°	19.88°	34.55°	-0.05	4.71

Gaussian profile (Skewness ≈ -0.05), indicating that unambiguous concepts ("Cat", "Sun") are passed through the layer with uniform, predictable transformations. In stark contrast, the Hard regime exhibits an explosion in skewness ($\gamma_1 = 4.71$). The "Long Tail" of this distribution reaches rotations of 34.55° , nearly double the inertial baseline. This provides quantitative evidence for the **Selective Steering Hypothesis**: PRISM conserves energy by letting unambiguous tokens coast, exerting significant computational work only on the specific subset of tokens that require disambiguation.

5.3 Mechanism Validation: Holographic Optical Learning

While the WMT14 results demonstrate the representational capacity of the architecture, a core theoretical motivation for PRISM is its compatibility with passive photonic hardware. To quantify the specific contribution of the holographic backpropagation mechanism, we conducted a rigorous ablation study comparing the *Learned Optical Layer* against a *Frozen Baseline* on a CIFAR-10 hardware simulation.

In the baseline configuration, the optical parameters were initialized randomly and kept fixed (frozen) throughout training, forcing the digital classifier to rely solely on random spectral projections (Random Scattering). Crucially, the digital readout head was fully trained in both configurations to isolate the specific contribution of optical feature optimization versus random scattering. Under identical noisy conditions (4-bit precision, stochastic intensity noise $\sigma \approx 0.01$), the Frozen baseline saturated at a test accuracy of **48.44%**, representing the theoretical capacity limit of the digital head operating on unoptimized inputs.

In contrast, utilizing our proposed holographic update rule allowed the model to reach **62.41%** accuracy. This results in a net **Optical Learning Gain of +13.97%**. Crucially, since the optical layer is strictly constrained to unity gain ($g \approx 1.0$), this performance uplift is mathematically decoupled from signal amplification (Rate Coding). The $\sim 14\%$ gap serves as empirical evidence that the gradient flow successfully optimized the phase delay parameters (ϕ), steering constructive interference toward semantically relevant features even in the absence of active gain.

6 Computational & Spectral Efficiency

Having established both the linguistic capacity (Section 5) and the physical feasibility (Section 5.3) of the PRISM architecture, we now turn to its computational profile. To validate the hypothesis that

spectral reasoning offers a metabolic advantage over attentional mechanisms, we analyze efficiency through two distinct lenses: structural cost (hardware) and metabolic leverage (information).

6.1 Structural Efficiency: Complexity and Density

The fundamental bottleneck of the standard Transformer is the Self-Attention mechanism, which scales quadratically $\mathcal{O}(L^2d)$. In contrast, PRISM’s Gated Harmonic Convolution relies on the Fast Fourier Transform (FFT), reducing the global mixing operation to log-linear time $\mathcal{O}(L \log L \cdot d)$.

Crucially, this spectral approach yields a higher "reasoning density." As detailed in Table 1, the PRISM encoder requires only **13.0M** parameters—a **31.2% reduction** compared to the 18.9M parameters of the standard Transformer encoder. By offloading complex feature mixing to the non-parametric spectral domain, the architecture reduces the memory footprint required for reasoning without sacrificing vocabulary capacity.

6.2 Spectral Efficiency: The "Metabolic" Ratio

Beyond hardware constraints, we investigate the *metabolic efficiency* of the network—defined as the ratio of semantic work performed to the "energy" (gate openness) consumed. We define the **Spectral Efficiency Score** (η) for a layer as:

$$\eta_{layer} = \frac{\Delta\theta}{\mu_{gate}} \tag{15}$$

where $\Delta\theta$ is the mean semantic phase rotation and μ_{gate} is the mean gate openness (synaptic permeability).

As illustrated in Figure 4 and detailed in Table 5, the network exhibits a "Cognitive Crossover" at Layer 2. In the deep layers (3-5), the model achieves massive semantic rotations ($\approx 17.38^\circ$) while strictly clamping gates ($\mu_{gate} \approx 0.16$). This yields a peak Spectral Efficiency Score of **102.98**, confirming that the model optimizes for reasoning by decoupling metabolic cost from semantic impact.

Table 5: **Spectral Efficiency Scores (η) by Layer.** Deep layers exhibit a six-fold increase in metabolic efficiency compared to the input layer, confirming the "High Leverage" hypothesis.

Layer Depth	Spectral Efficiency (η)
0	16.62
1	30.44
2	38.91
3	59.15
4	70.65
5	102.98

6.3 Practical Training Efficiency: The Cost of Rigidity

While theoretical analysis suggests FNet should be computationally lighter due to real-valued operations, empirical training metrics reveal a different reality. The spectral filters in standard FNet are length-dependent, necessitating fixed-length padding (Section 3.3) to maintain spectral consistency. This introduces significant computational waste when processing variable-length text.

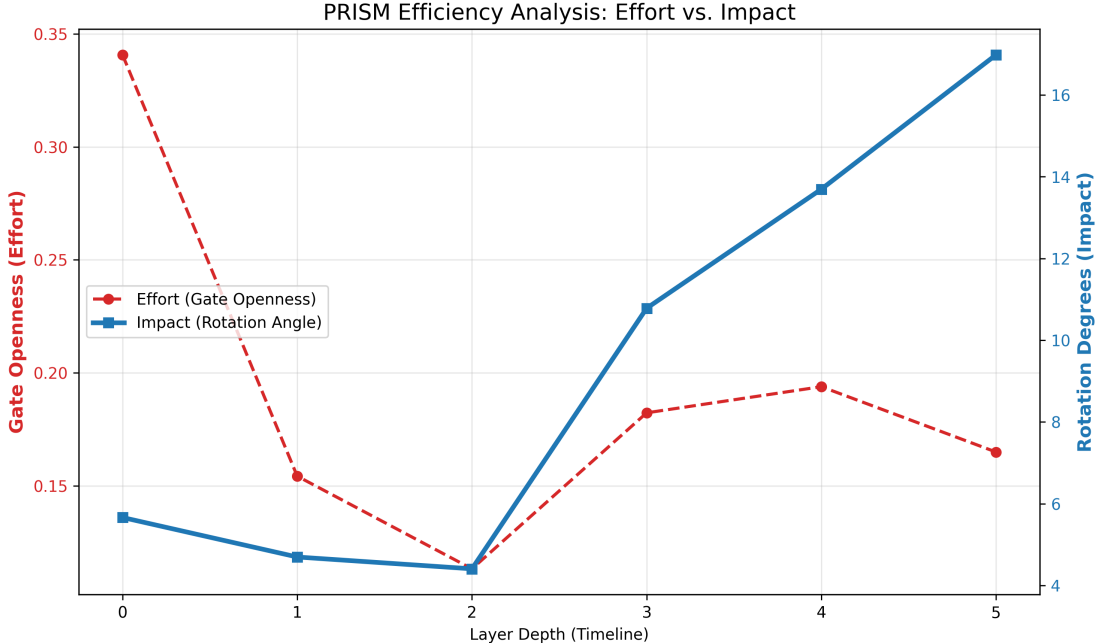


Figure 4: **The Metabolic Crossover.** Analysis of computational effort (Gate Openness, Red) versus semantic impact (Phase Rotation, Blue). While early layers expend high energy for low impact, a crossover at Layer 2 leads to a high-leverage regime ($\eta > 100$) in deep layers, where the network achieves massive semantic steering with minimal gate activity.

In contrast, PRISM’s Gated Harmonic Convolutions are compatible with **Dynamic Bucketing**, allowing the model to process batches with minimal padding. As a result, despite utilizing computationally heavier complex-valued kernels, **PRISM reduces VRAM usage by $\approx 2\times$ and increases training throughput by $\approx 2\times$** compared to the FNet baseline on the WMT14 task. This demonstrates that *algorithmic flexibility* (the ability to handle variable lengths) yields greater practical efficiency than *operation-level simplicity*. Crucially, this speedup is achieved using standard, unoptimized PyTorch complex kernels; We hypothesize that specialized CUDA implementations of the Harmonic Convolution could further widen this performance gap. Furthermore, the mathematical isomorphism between PRISM’s spectral mixing and the Orthogonal Frequency-Division Multiplexing (OFDM) schemes used in 5G telecommunications suggests a direct hardware path: PRISM is uniquely suited for deployment on existing Digital Signal Processors (DSPs) optimized for radio-frequency FFT workloads, potentially unlocking edge-AI capabilities on commodity telecom silicon that are inaccessible to standard Transformers.

6.4 Heterogeneous Inference Strategy: The “Digital Twin” Protocol

A critical challenge in Optical Neural Networks (ONNs) is the difficulty of computing physical gradients in situ. PRISM addresses this via a “Digital Twin” training protocol: the model is trained digitally using phase-preserving constraints that mirror physical laws, and the learned parameters are subsequently imprinted onto the optical hardware.

We define two distinct inference regimes based on the downstream task:

1. Hybrid Regime (Generative Tasks): For sequence-to-sequence tasks like WMT14, we employ the architecture validated in this work (‘PRISMHybrid’).

- **The Optical Encoder** processes the global context via wave propagation ($O(1)$ time).
- **The Digital Decoder** handles the autoregressive token generation. This leverages the precision of digital electronics for sequential probability sampling (Softmax), which remains challenging in purely analog systems.

2. Pure Optical Regime (Discriminative Tasks): For sequence classification tasks (e.g., Genomic Classification, Sentiment Analysis), the Digital Decoder is rendered unnecessary. The final spectral state of the PRISM Encoder can be mapped directly to class probabilities via a physical intensity readout layer. This enables an end-to-end passive inference pipeline that operates entirely within the optical domain, bypassing the digital bottleneck completely.

6.5 Theoretical Photonic Advantage

While algorithmic innovations like Mamba [Gu and Dao \(2024\)](#) and Hyena [Poli et al. \(2023\)](#) achieve linear scaling on digital hardware, they remain bound by the fundamental energy costs of active transistor switching (~ 10 pJ/MAC). PRISM is designed to transcend this barrier. In a realized optical implementation, the core spectral mixing operation—performed digitally via FFT ($O(N \log N)$)—is physically executed by a lens at the speed of light. As detailed in Table 6, this shifts the computational complexity of global token mixing from a function of sequence length N to a constant propagation time $O(1)$, independent of input resolution. Furthermore, the Iso-Energetic constraint allows the system to operate in a "Passive Regime," where computation consumes negligible power compared to the active recurrence required by State-Space Models.

Table 6: **Theoretical Efficiency Landscape.** Comparison of mixing complexity and energy mechanisms across architectural paradigms. While Mamba and Hyena optimize for GPU memory hierarchies, PRISM optimizes for physical wave propagation. (*Denotes effective complexity in an optical 4f system).

Architecture	Mixing Mechanism	Time Complexity	Energy Regime	Physical Substrate
Transformer	Self-Attention	$O(N^2)$	Active (High)	Digital (GPU)
Hyena / FNet	Digital FFT	$O(N \log N)$	Active (Med)	Digital (GPU)
Mamba (SSM)	Recurrent Scan	$O(N)$	Active (Low)	Digital (GPU)
PRISM (Ours)	Optical Diffraction	$O(1)^*$	Passive (Iso-Energetic)	Photonic (Analog)

7 Discussion

7.1 Physical Admissibility: Why Standard Spectral Models Fail in Optics

While architectures like FNet leverage the Fast Fourier Transform (FFT) for token mixing, they remain fundamentally distinct from PRISM in terms of physical admissibility. Standard spectral models operate under the Rate Coding paradigm, where token identity is often disentangled via unbounded amplitude variations. In a passive optical system, such operations would violate the Law of Conservation of Energy, requiring active amplification at every layer to prevent signal decay or explosion.

In contrast, PRISM enforces a strict Iso-Energetic constraint (Gain ≈ 1.0). By restricting the network to phase-only modulation, we ensure that the model operates within the “unitary budget” of a laser source. Our results (Table 2) reveal a critical insight: the FNet baseline, which operates without energy restrictions, achieves a COMET score of 0.805, while PRISM achieves 0.799. This implies that the “cost” of physical admissibility is negligible.

Even if both architectures are operating near the saturation limit of the WMT14 dataset, the fact that PRISM reaches this ceiling under strict Unitary constraints—while FNet requires unbounded amplitude—suggests that magnitude variation is likely a **compensatory mechanism** required by real-valued spectral models. While FNet must utilize amplitude to encode feature salience (due to its lack of phase capacity), PRISM demonstrates that complex-valued phase manipulation is a sufficient and more physically admissible alternative for semantic reasoning.

Consequently, while FNet utilizes the Fourier Transform as a mathematical shortcut on GPUs, PRISM utilizes it as a simulation of physical lensing, making it the only candidate among spectral architectures capable of native execution on passive photonic interconnects without requiring extensive electro-optical conversion overhead.

7.2 Architectural Phylogeny: Spectral vs. State-Space

The recent surge in linear-time architectures, such as Mamba and Hyena, represents a triumph of hardware-aware engineering, optimizing recurrent states for the memory hierarchy of modern GPUs. However, these State-Space Models (SSMs) are inherently causal and recurrent, designed primarily for auto-regressive decoding. PRISM occupies a different phylogenetic niche. It is a native bidirectional encoder designed for spectral global reasoning. Unlike Mamba, which compresses context into a fixed-size recurrent state, PRISM maintains a holographic view of the sequence via the frequency domain. This distinction is crucial for non-causal tasks such as genomic sequence modeling or bidirectional translation, where “future” tokens are physically available and essential for resolving local ambiguity. Furthermore, while Hyena approximates long convolutions via FFTs, it relies on unconstrained filters that lack the phase-conjugate symmetry required for holographic optical learning.

7.3 Strategic Scaling and Domain Applicability

In an era driven by the “Scale is All You Need” dogma (Kaplan et al., 2020), a natural critique is the relatively modest parameter count of our experimental prototype ($\sim 70\text{M}$). However, we argue that for novel, physically-grounded architectures, immediate parameter scaling is a premature optimization. The primary barrier to the adoption of Optical Neural Networks is not representational capacity, but **physical realizability** and hardware-software co-design.

Our experimental focus on Natural Language (WMT14) was driven by **Mechanistic Interpretability**. Unlike genomics or raw signals, language offers rich, high-level semantic structures (e.g., synonymy, polysemy) that are human-interpretable. This allowed us to explicitly validate the *Phase-Coding Hypothesis* via the Semantic Phase Compass (Section 5.1), confirming that the network encodes meaning in phase angles—a verification that would be opaque in abstract domains like DNA sequence modeling.

Moving forward, the scaling trajectory of PRISM should not blindly mimic Large Language Models (LLMs). Instead, the next phase of validation should target **Long-Context, Narrow-Width** regimes similar to **HyenaDNA** Nguyen et al. (2023), where the $\mathcal{O}(N \log N)$ spectral core provides a decisive algorithmic advantage over quadratic Attention. Our priority remains securing the physical substrate (Section 5.3) first; scaling parameters before solving the hardware constraints

would yield merely another digital simulation, rather than a blueprint for photonic intelligence.

8 Future Work

8.1 Silicon Photonic Realization

Having validated the architecture’s theoretical capacity on WMT14 and its mechanistic trainability via holographic backpropagation simulations (Section 3.4), the immediate frontier is physical instantiation. Future work will focus on porting the PRISM architecture to programmable silicon photonic processors. The Iso-Energetic nature of the model allows for the direct mapping of weights to phase-shifters (e.g., Mach-Zehnder Interferometers), potentially enabling inference speeds limited only by the propagation delay of light through the waveguide, offering orders-of-magnitude improvements in latency and energy efficiency over electronic counterparts.

8.2 Genomics and Long-Context Reasoning

While WMT14 serves as a robust linguistic benchmark, the $O(N \log N)$ spectral core of PRISM is mathematically destined for sequence lengths that cripple quadratic Attention mechanisms ($L > 100k$). Biological sequences, such as DNA and proteins, are naturally encoded in non-causal, bidirectional structures where distal regulatory elements interact across millions of base pairs. We intend to scale PRISM to these genomic domains, testing the hypothesis that the harmonic patterns of the "Phase-Coding" latent space align more closely with the oscillatory nature of biological information storage than scalar vectors.

8.3 Native RF & Telecommunications Intelligence

Beyond biological sequences, the PRISM architecture shares a fundamental mathematical isomorphism with modern telecommunications protocols. 5G and 6G signals are typically represented as complex-valued In-phase and Quadrature (IQ) data ($I + iQ$). Standard deep learning approaches often treat these components as independent real-valued channels, ignoring the intrinsic phase relationships that encode modulation information (e.g., QAM, PSK).

PRISM represents a paradigm shift for Radio Frequency (RF) machine learning: it is capable of ingesting raw IQ data natively without feature engineering. By processing the signal in its natural complex domain, PRISM could theoretically enable ultra-efficient tasks such as Neural Beamforming, Modulation Classification, and Channel Estimation directly on the DSP hardware, bridging the gap between classical signal processing and modern AI.

9 Conclusion

We have presented PRISM, a sequence modeling architecture that aligns deep learning with the physical constraints of wave mechanics. By enforcing an Iso-Energetic Unity Gain regime, we demonstrated that semantic reasoning does not require the metabolically expensive amplitude modulation inherent to Rate Coding; rather, it can be fully realized through the interference of complex-valued phasors.

Empirically, PRISM achieves parity with unconstrained spectral baselines (FNet) on the WMT14 benchmark (0.799 vs 0.805 COMET) while utilizing 11.5% fewer parameters and enabling passive optical inference. Furthermore, our mechanistic analysis revealed that the network naturally discovers a "Phase Steering" strategy, selectively rotating polysemous tokens while leaving unambiguous

concepts in an inertial state. These results suggest that the next leap in efficiency may not come from smaller transistors, but from architectures that treat light not as a medium for transmission, but as a substrate for reasoning.

Code Availability

To facilitate reproducibility and further research into optical neural architectures, we release the complete PyTorch implementation of PRISM, including the complex-valued training kernels and the holographic optical simulation environment.

- **GitHub Repository:** <https://github.com/AlperYildirim1/Language-as-Waves>
- **Archival DOI (Zenodo):** [10.5281/zenodo.17332647](https://doi.org/10.5281/zenodo.17332647)

The repository includes scripts for the WMT14 translation task, the CIFAR-10 optical ablation study, and the mechanistic phase analysis tools used in Section 5.

Acknowledgments

We acknowledge the use of Large Language Models (LLMs) for assistance with PyTorch debugging, LaTeX typesetting, and narrative refinement. The authors retain full responsibility for the scientific accuracy, experimental methodology, and final conclusions presented in this work.

References

- Martin Arjovsky, Amar Shah, and Yoshua Bengio. Unitary evolution recurrent neural networks. In *Proceedings of the 33rd International Conference on International Conference on Machine Learning - Volume 48*, ICML'16, page 1120–1128. JMLR.org, 2016.
- Selen Atasoy, Isaac Donnelly, and Joel Pearson. Human brain networks function in connectome-specific harmonic waves. *Nature Communications*, 7(1):10340, 2016.
- Ondřej Bojar, Christian Buck, Christian Federmann, Barry Haddow, Philipp Koehn, Johannes Leveling, Christof Monz, Pavel Pecina, Matt Post, Herve Saint-Amand, et al. Findings of the 2014 workshop on statistical machine translation. In *Proceedings of the ninth workshop on statistical machine translation*, pages 12–58, 2014.
- Gustavo Deco, Yonatan Sanz Perl, and Morten L Kringelbach. Complex harmonics reveal low-dimensional manifolds of critical brain dynamics. *Physical Review E*, 111(1):014410, 2025.
- Olesia Dogonashva, Denis Zakharov, Anne-Lise Giraud, and Boris Gutkin. Neuro-oscillatory models of cortical speech processing. *arXiv preprint arXiv:2502.12935*, 2025.
- Pascal Fries. A mechanism for cognitive dynamics: neuronal communication through neuronal coherence. *Trends in cognitive sciences*, 9(10):474–480, 2005.
- Anne-Lise Giraud and David Poeppel. Cortical oscillations and speech processing: emerging computational principles and operations. *Nature neuroscience*, 15(4):511–517, 2012.
- Joseph W Goodman. *Introduction to Fourier Optics*. Roberts and Company Publishers, 2005.

- Albert Gu and Tri Dao. Mamba: Linear-time sequence modeling with selective state spaces, 2024. URL <https://openreview.net/forum?id=AL1fq05o7H>.
- John J Hopfield and Carlos D Brody. What is a moment? transient synchrony as a collective mechanism for spatiotemporal integration. *Proceedings of the National Academy of Sciences*, 98(3):1282–1287, 2001.
- Enhao Huang, Zhiyu Zhang, Tianxiang Xu, Chunshu Xia, and Kaichun Hu. Holographic transformers for complex-valued signal processing. *arXiv preprint arXiv:2509.19331*, 2025.
- Jared Kaplan, Sam McCandlish, Tom Henighan, Tom B Brown, Benjamin Chess, Rewon Child, Scott Gray, Alec Radford, Jeffrey Wu, and Dario Amodei. Scaling laws for neural language models. *arXiv preprint arXiv:2001.08361*, 2020.
- Diederik P Kingma and Jimmy Ba. Adam: A method for stochastic optimization. In *International Conference on Learning Representations (ICLR)*, 2015. URL <http://arxiv.org/abs/1412.6980>.
- Alex Krizhevsky, Geoffrey Hinton, et al. Learning multiple layers of features from tiny images. Technical report, University of Toronto, Toronto, Ontario, 2009.
- Sachin Kumar and Yulia Tsvetkov. Von mises-fisher loss for training sequence to sequence models with continuous outputs. In *International Conference on Learning Representations*, 2019.
- Simon B Laughlin and Terrence J Sejnowski. Communication in neuronal networks. *Science*, 301(5641):1870–1874, 2003.
- James Lee-Thorp, Joshua Ainslie, Ilya Eckstein, and Santiago Ontanon. Fnet: Mixing tokens with fourier transforms. In *Proceedings of the 2022 Conference of the North American Chapter of the Association for Computational Linguistics: Human Language Technologies*, pages 4296–4313, 2022.
- Xing Lin, Yair Rivenson, Nezih T Yardimci, Muhammed Veli, Mona Jarrahi, and Aydogan Ozcan. All-optical machine learning using diffractive deep neural networks. *Science*, 361(6406):1004–1008, 2018.
- Ilya Loshchilov and Frank Hutter. Decoupled weight decay regularization. In *International Conference on Learning Representations*, 2019. URL <https://openreview.net/forum?id=Bkg6RiCqY7>.
- Eric Nguyen, Michael Poli, Marjan Faizi, Armin Thomas, et al. HyenaDNA: Long-range genomic sequence modeling at single nucleotide resolution. In *Advances in Neural Information Processing Systems*, volume 36, 2023.
- Toan Q Nguyen and Julian Salazar. Transformers without tears: Improving the normalization of self-attention. *arXiv preprint arXiv:1910.05895*, 2019.
- Michael Poli, Stefano Massaroli, Eric Nguyen, Daniel Y Fu, Tri Dao, Stephen Baccus, Yoshua Bengio, Stefano Ermon, and Christopher Ré. Hyena hierarchy: Towards larger convolutional language models. In *International Conference on Machine Learning*, pages 28043–28078. PMLR, 2023.
- Ricardo Rei, José G. C. de Souza, Duarte Alves, Chrysoula Zerva, Ana C Farinha, Taisiya Glushkova, Alon Lavie, Luisa Coheur, and André F. T. Martins. COMET-22: Unbabel-IST 2022 submission for the metrics shared task. In *Proceedings of the Seventh Conference on Machine Translation*

- (WMT), pages 578–585, Abu Dhabi, United Arab Emirates (Hybrid), December 2022. Association for Computational Linguistics.
- Jianlin Su, Yu Lu, Shengfeng Pan, Ahmed Murtadha, Bo Wen, and Yunfeng Liu. Roformer: Enhanced transformer with rotary position embedding. *Neurocomputing*, 568:127063, 2024.
- Ian Tenney, Dipanjan Das, and Ellie Pavlick. Bert rediscovers the classical nlp pipeline. In *Proceedings of the 57th Annual Meeting of the Association for Computational Linguistics*, pages 4593–4601, 2019.
- Jörg Tiedemann and Santhosh Thottingal. Opus-mt-building open translation services for the world. In *Proceedings of the 22nd Annual Conference of the European Association for Machine Translation*, pages 479–480, 2020.
- Chiheb Trabelsi, Olexa Bilaniuk, Ying Zhang, Dmitriy Serdyuk, Sandeep Subramanian, Joao Felipe Santos, Soroush Mehri, Negar Rostamzadeh, Yoshua Bengio, and Christopher J Pal. Deep complex networks. In *International Conference on Learning Representations*, 2018. URL <https://openreview.net/forum?id=H1T2hmZAb>.
- Ashish Vaswani, Noam Shazeer, Niki Parmar, Jakob Uszkoreit, Llion Jones, Aidan N Gomez, Łukasz Kaiser, and Illia Polosukhin. Attention is all you need. In *Advances in Neural Information Processing Systems*, volume 30, 2017.
- Kelvin Wagner and Demetri Psaltis. Multilayer optical learning networks. *Applied Optics*, 26(23): 5061–5076, 1987.
- Benyou Wang, Donghao Zhao, Christina Lioma, Qiuchi Li, Peng Zhang, and Jakob Grue Simonsen. Encoding word order in complex embeddings. In *International Conference on Learning Representations (ICLR)*, 2020. URL <https://openreview.net/forum?id=Hke-Wp4YDB>.

Table 7: **Comprehensive Phase Locking Statistics.** Aggregate analysis of R values for $N = 67$ word pairs. Note that the maximum coherence for Synonyms (0.45) is significantly higher than the random baseline maximum (0.12).

Type	N	Mean	Std	Min	25%	50%	75%	Max
Synonym	35	0.198	0.090	0.023	0.138	0.190	0.257	0.455
Antonym	13	0.117	0.056	0.037	0.087	0.110	0.142	0.223
Random	19	0.077	0.031	0.002	0.062	0.073	0.101	0.125

A Detailed Phase Statistics

Table 7 presents the complete descriptive statistics for the Mean Resultant Length (R) distributions across the three semantic categories tested in the Phase Compass experiment.